Supplement of

Aqueous-phase chemistry of glyoxal with multifunctional reduced nitrogen compound: A potential missing route of secondary brown carbon

Yuemeng Ji[1,2], Zhang Shi[1,2], Wenjian Li[1,2], Jiaxin Wang[1,2], Qiuju Shi[1,2], Yixin Li[3], Lei Gao[1,2], Ruize Ma[1,2], Weijun Lu[2], Lulu Xu[1,2], Yanpeng Gao[1,2], Guiying Li[1,2], Taicheng An[1,2]

[1]Guangdong Key Laboratory of Environmental Catalysis and Health Risk Control, Guangdong-Hong Kong-Macao Joint Laboratory for Contaminants Exposure and Health, Institute of Environmental Health and Pollution control, Guangdong University of Technology, Guangzhou 510006, China;

[2]Guangzhou Key Laboratory of Environmental Catalysis and Pollution Control, Key Laboratory of City Cluster Environmental Safety and Green Development, School of Environmental Science and Engineering, Guangdong University of Technology, Guangzhou 510006, China.

[3]Department of Chemistry, University of California Irvine, Irvine, CA 92697, USA

Correspondence to: Prof. Taicheng An (antc99@gdut.edu.cn)

Experiments:

Chemicals and Reagents

The chemicals purchased from Sigma Aldrich are as followings: glyoxal (GL, 40 wt% solution), ammonium sulfate (AS, > 99%), monoethanolamine (MEA, > 99%). Sulfuric acid (> 98%) and sodium hydroxide (> 96%) were purchased from Guangzhou Chemical Reagent Factory (Guangzhou, China). High-purity deionized water (18.2 MΩ cm) (Millipore Corp., USA) were used for dissolution and dilution.

Mass spectrometry and chromatographic conditions

The selected chromatographic column was Hypersil GOLD C18 (100 × 2.1 mm, 1.9 μm). The injection volume was 1 μL and the eluents were ultrapure water (eluent A) and acetonitrile (eluent B). The flow rate of mobile phase was 0.25 mL min^{-1} with a gradient descripted as follows: First, starting with 2% B for 2 min, increasing to 95% B at 15 min, isocratic elution for 3 min, then decreasing to 2% B in 0.1 min and finally maintain 2% B to 20 min. Mass spectrometry detectors were equipped with a HESI source and set under the parameters as listed followingly: 4 kV spray voltage, 30 units of sheath gas flow, 10 units of auxiliary gas flow, 320 °C capillary temperature and 350 °C auxiliary gas heater temperature. MS mode was set with a scan range of 50-750 m/z with a resolution of 70000. While in MS^2 mode, the resolution was 17500.

Detailed description of rate constants

The rate constant (k) with the $\Delta G^{\ddagger}$ value was calculated using Conventional Transition State theory (TST) (Eyring, 1935; Galano and Alvarez-Idaboy, 2009; Gao et al., 2014; Ji et al., 2022) as follows:

$$k_t = \sigma \frac{k_B T}{h} \exp\left(\frac{-\Delta G^{\ddagger}}{RT}\right) \quad (1)$$

where k_B and h are the Boltzmann and Planck constants, respectively; $\Delta G^{\ddagger}$ represents the activation energy of the reaction with the thermodynamic contribution corrections and solvent cage effects taken into consideration, and σ represents the reaction path degeneracy.

To simulate realistic conditions in the solution, the solvent cage effect, which was proposed by Okuno (Okuno, 1997), is incorporated into the free volume theory. Gibbs free energy is corrected by the expression as follows:

$$\Delta G_{sol}^{FV} \cong \Delta G_{sol}^{0} - RT\{\ln[n10^{(2n-2)}] - (n\text{-}1)\} \quad (2)$$

where ΔG_{sol}^{0} is the Gibbs free energy of the reaction in the solution and n denotes the molecule number of the reaction. According to expression (2), the cage effects in the solution cause a decrease in the Gibbs free energy by 2.54 kcal mol^{-1} for bimolecular reactions occurring at 298.15 K.

Thus, the apparent rate constant (k) obtained from the diffusion-limit effect (Collins and Kimball, 1949) can be calculated by the formula as follows:

$$k = \frac{k_t k_d}{k_t + k_d} \quad (3)$$

where the k_t is the thermal rate constant from expression (1). The diffusion-limited rate constant (k_d) for a bimolecular reaction is calculated as follows:

$$k_D = 4\pi R D_{AB} N_A \quad (4)$$

where R is the reaction distance, N_A denotes the Avogadro number, and D_{AB} is the mutual diffusion coefficient of the reactants A and B. According to the previous study, D_{AB} has been calculated from D_A and D_B (Truhlar, 1985) which have been estimated from the Stokes–Einstein approach (Einstein, 1905) listed in expression (5):

$$D = \frac{k_B T}{6\pi\eta\alpha} \quad (5)$$

where k_B is the Boltzmann constant, T is the temperature, η denotes the viscosity of the solvent, which is water in our case ($\eta = 8.9 \times 10^{-4}$ Pa s), and α is the radius of the solute.

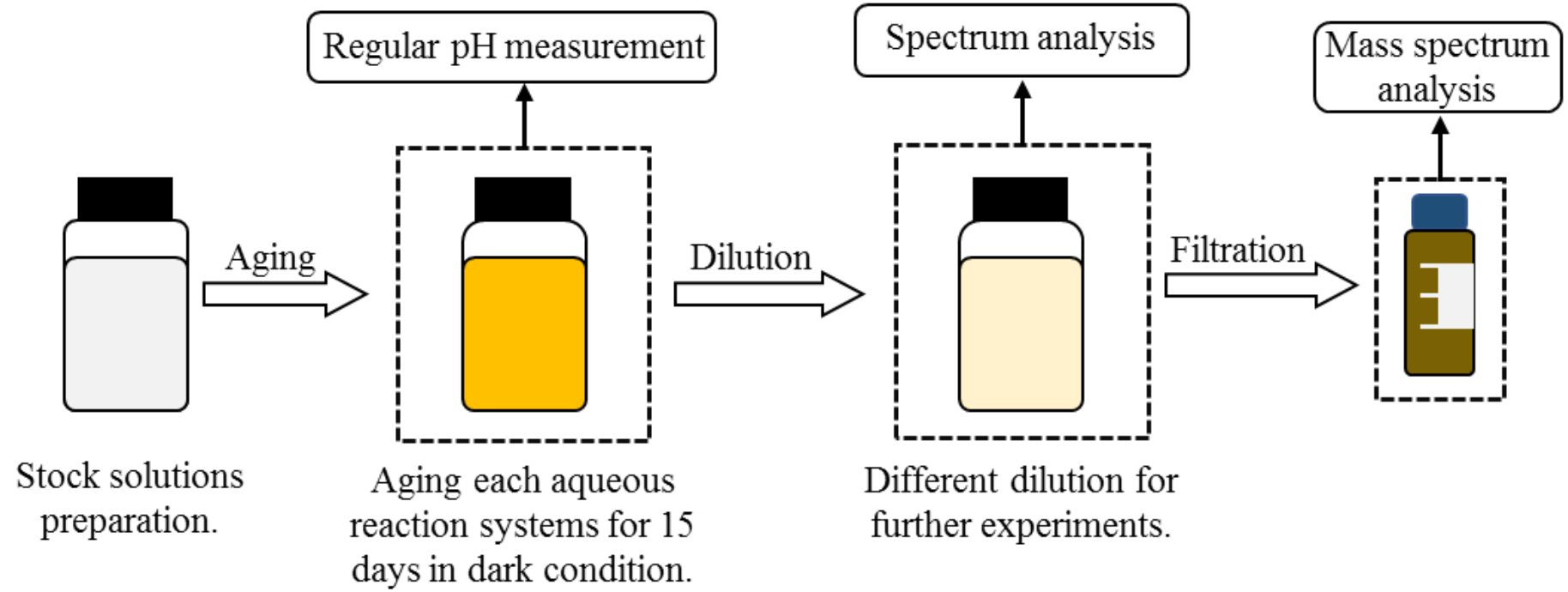

Figure S1. Experimental procedures.

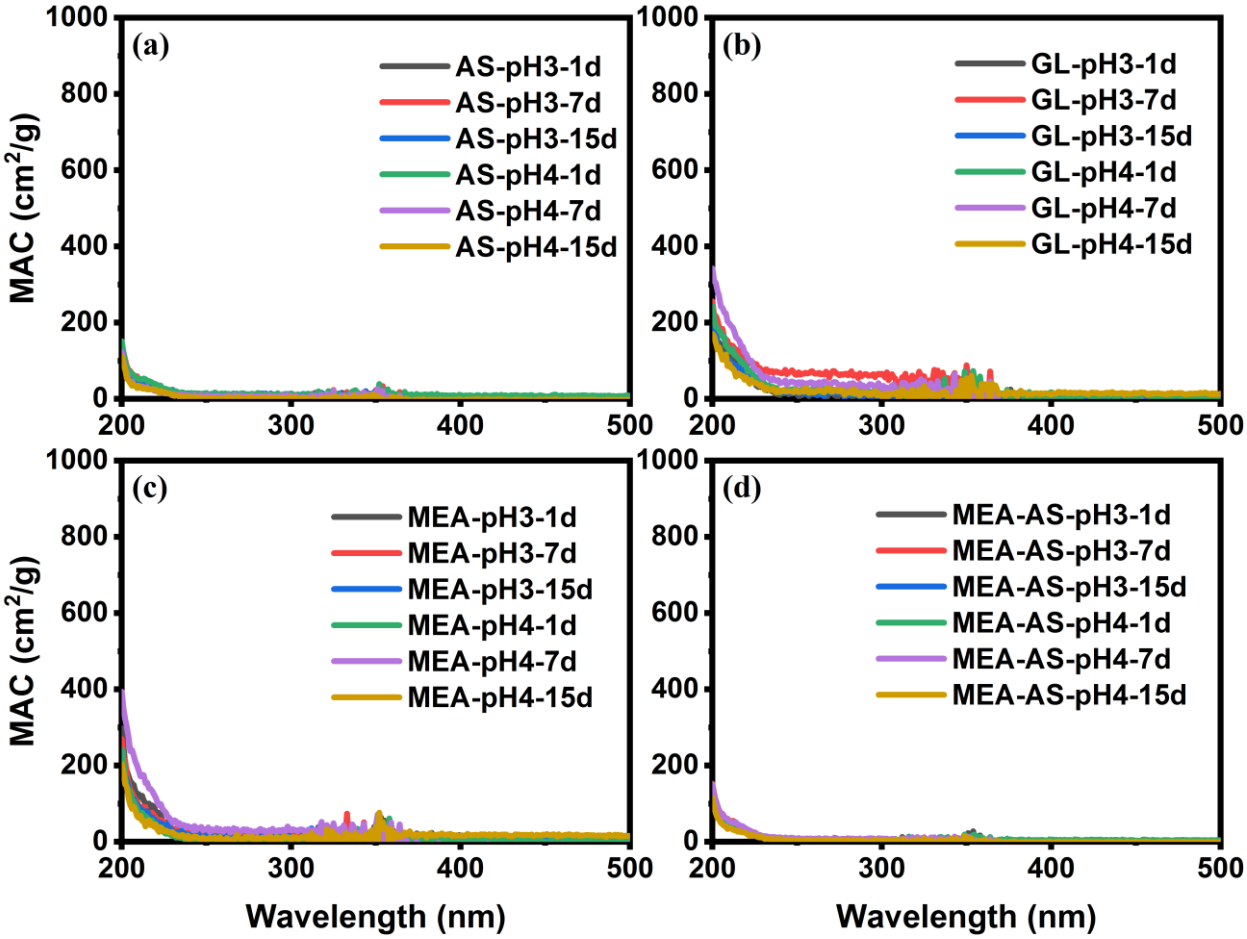

Figure S2. The MAC values of 1M (a) AS, (b) GL, (c) MEA and (d) MEA-AS solutions placed in dark over a time scale of 15 d.

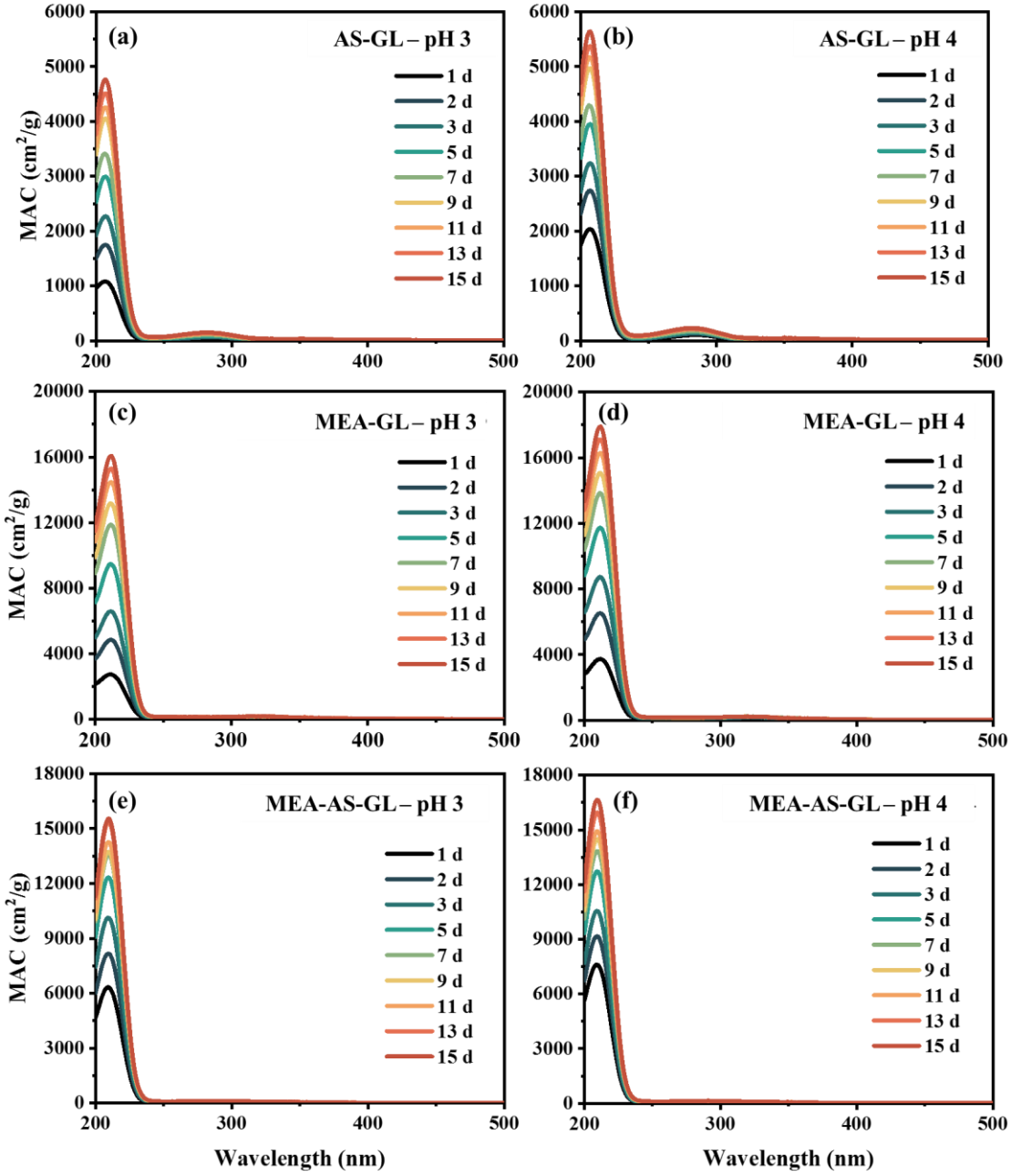

Figure S3. The MAC values for AS-GL (a and b), MEA-GL (c and d) and MEA-AS-GL (e and f) mixtures at the initial pH of 3 and 4 over a time scale of 15 d.

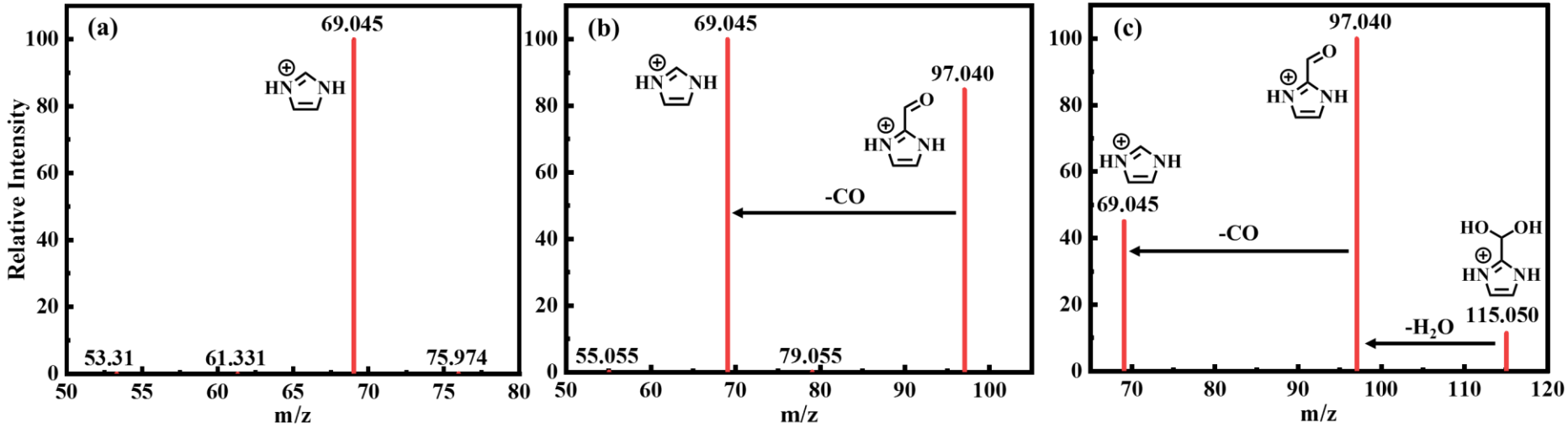

Figure S4. MS^2 spectrums for m/z (a) 69.045, (b) 97.040 and (c) 115.050 with parent ions and fragments labeled on peaks (red). A few fragments with low intensity are removed.

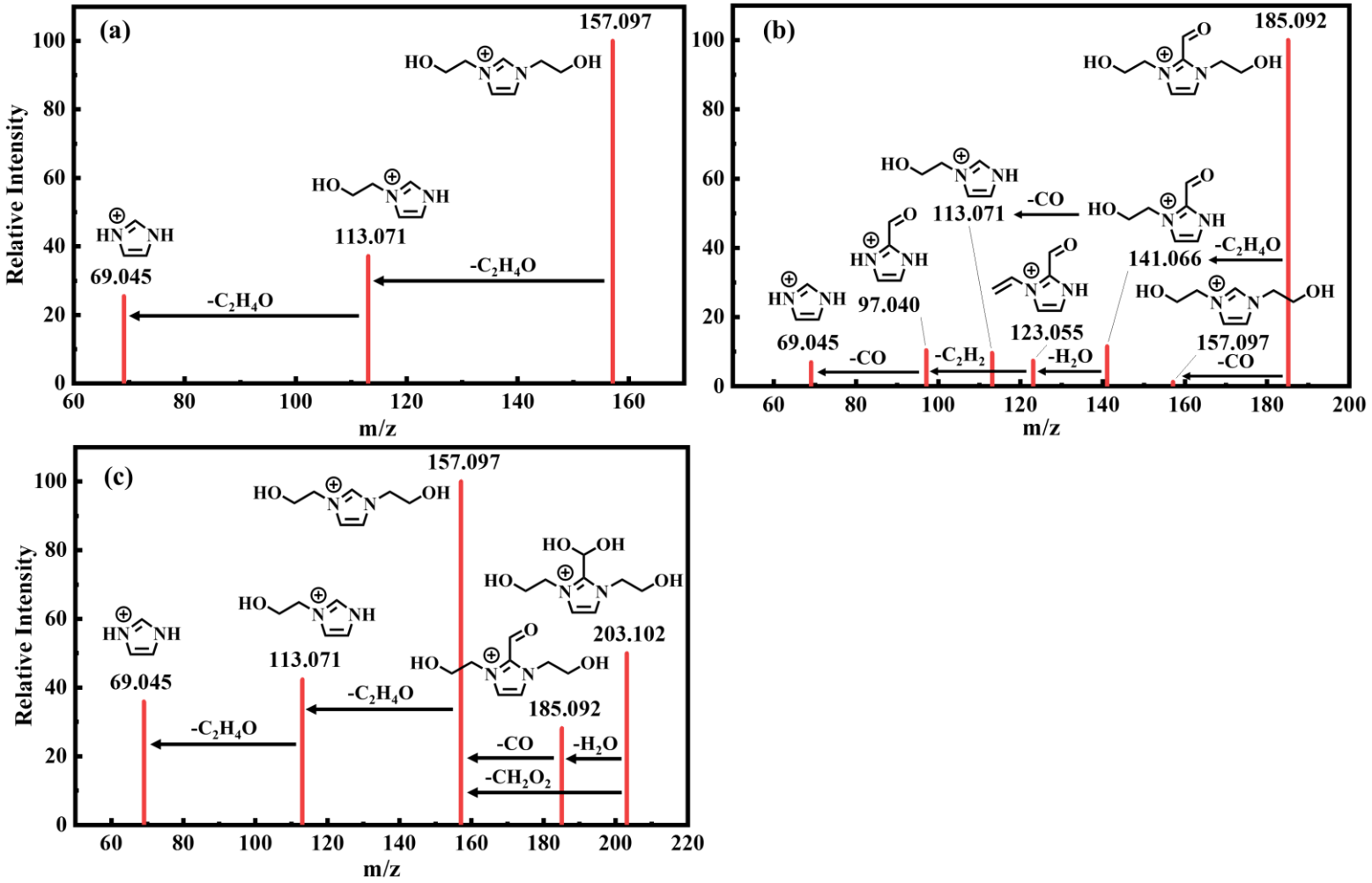

Figure S5. MS^2 spectrums for m/z (a) 157.097, (b) 185.092 and (c) 203.102 with parent ions and fragments labeled on peaks (red). A few fragments with low intensity are removed.

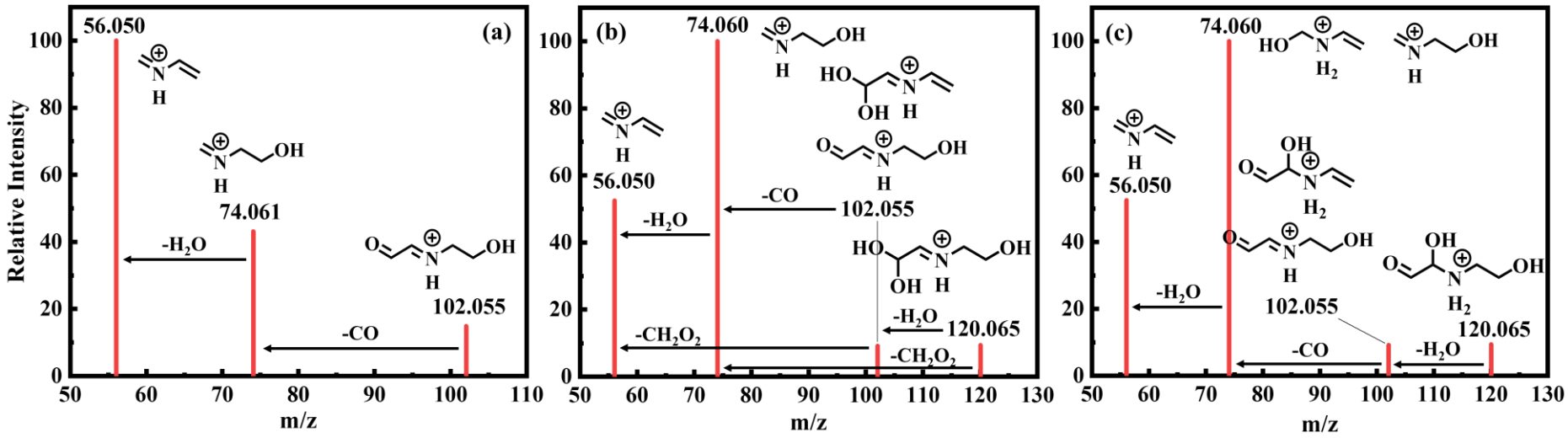

Figure S6. MS^2 spectrums for m/z (a) 102.055, (b) 120.065 and (c) its isomer with parent ions and fragments labeled on peaks (red). A few fragments with low intensity are removed.

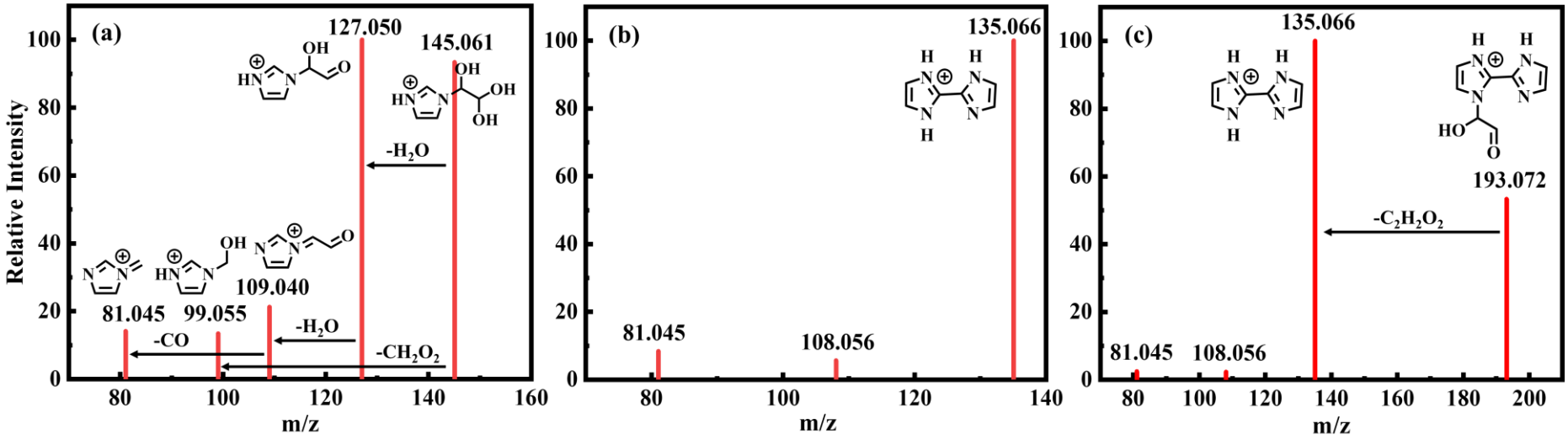

Figure S7. MS^2 spectrums for m/z (a) 145.061, (b) 135.066 and (c) 193.072 with parent ions and fragments labeled on peaks (red). A few fragments with low intensity are removed.

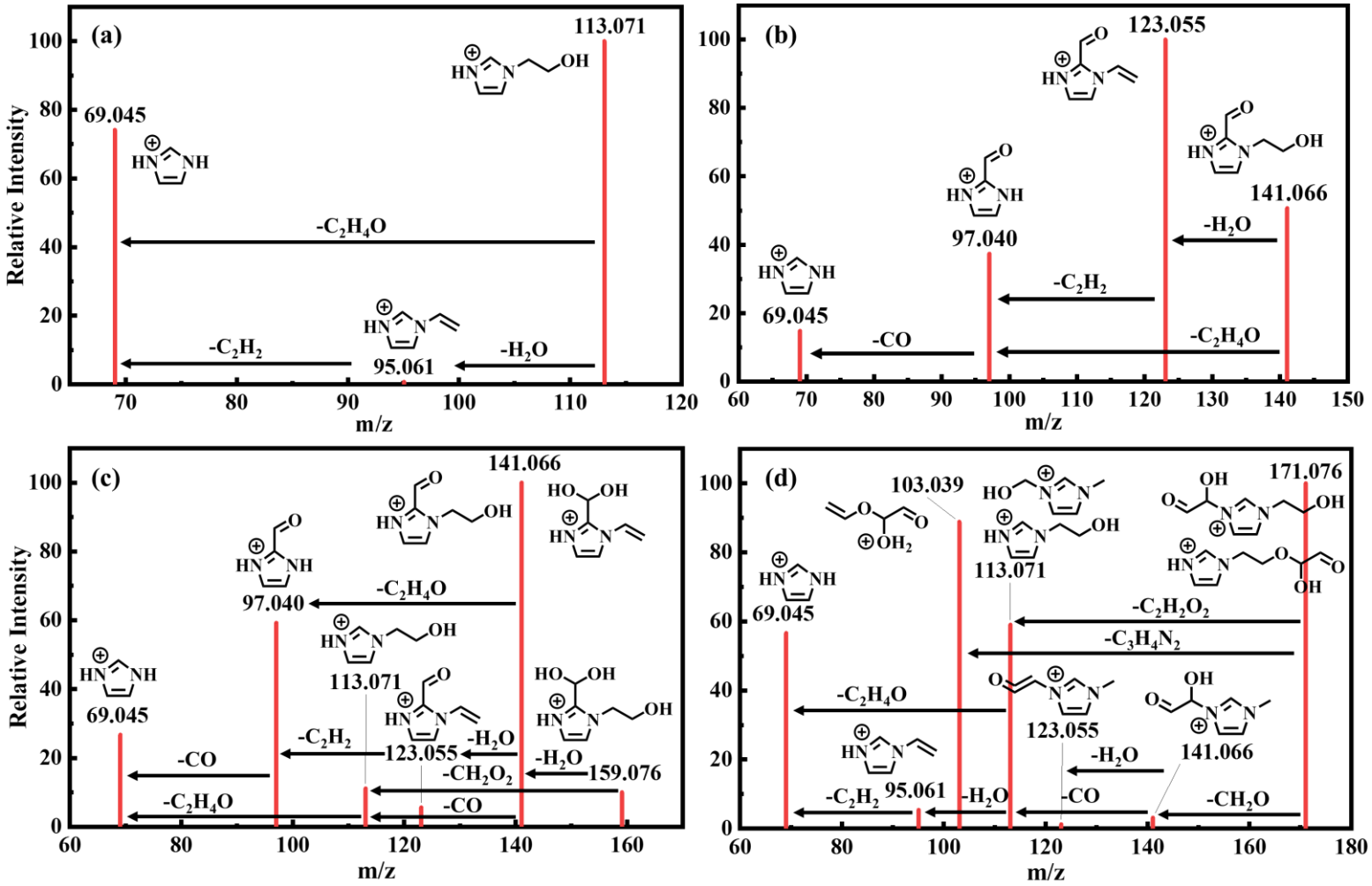

Figure S8. MS^2 spectrums for m/z (a) 113.071, (b) 141.066, (c) 159.076 and (d) 171.076 with parent ions and fragments labeled on peaks (red). A few fragments with low intensity are removed.

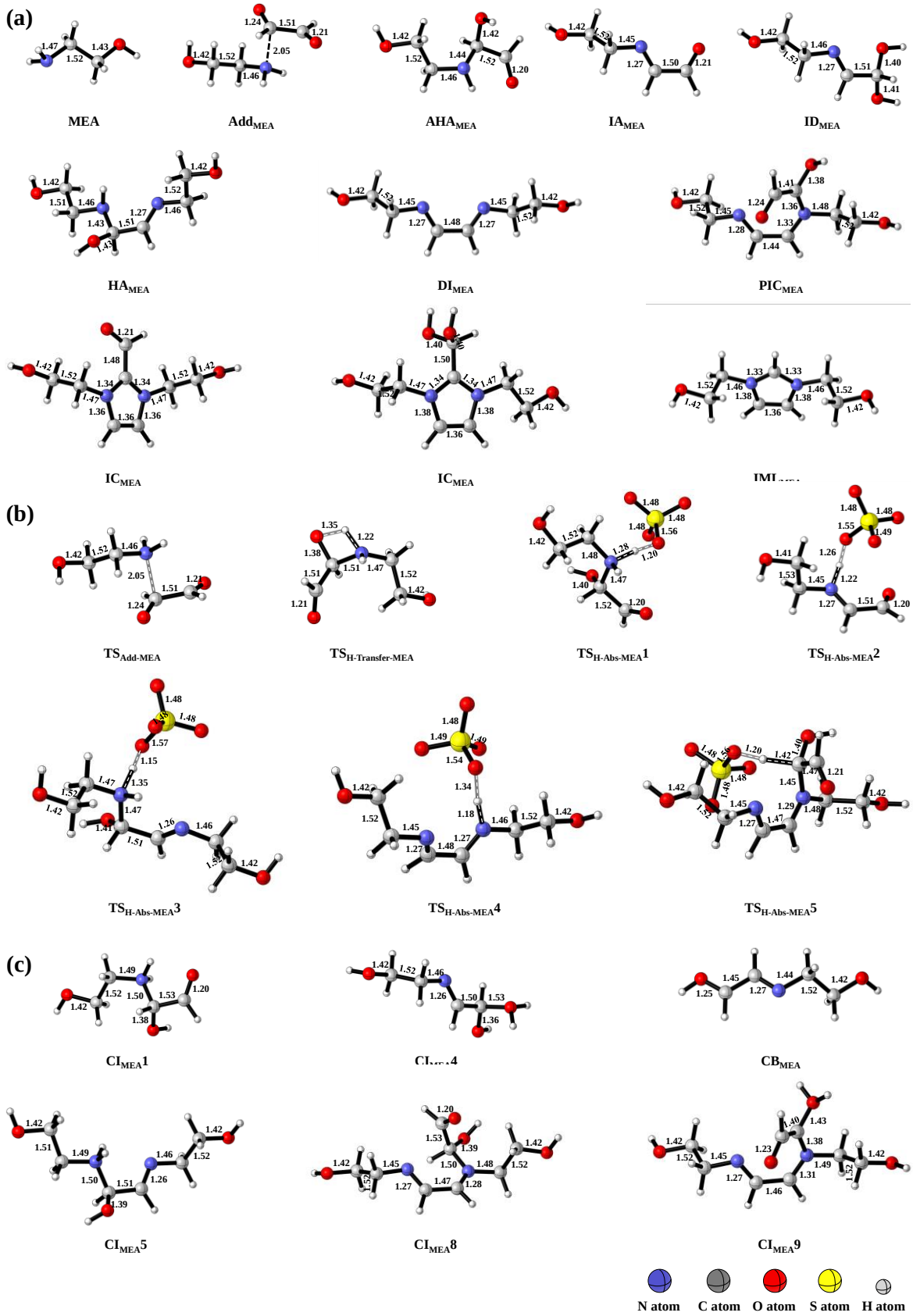

Figure S9. The optimized geometries of SPs including products (a), TSs (b) and CIs(c) in MEA-GL mixture. The structures were visualized by CYLview 1.0b software (Cylview).

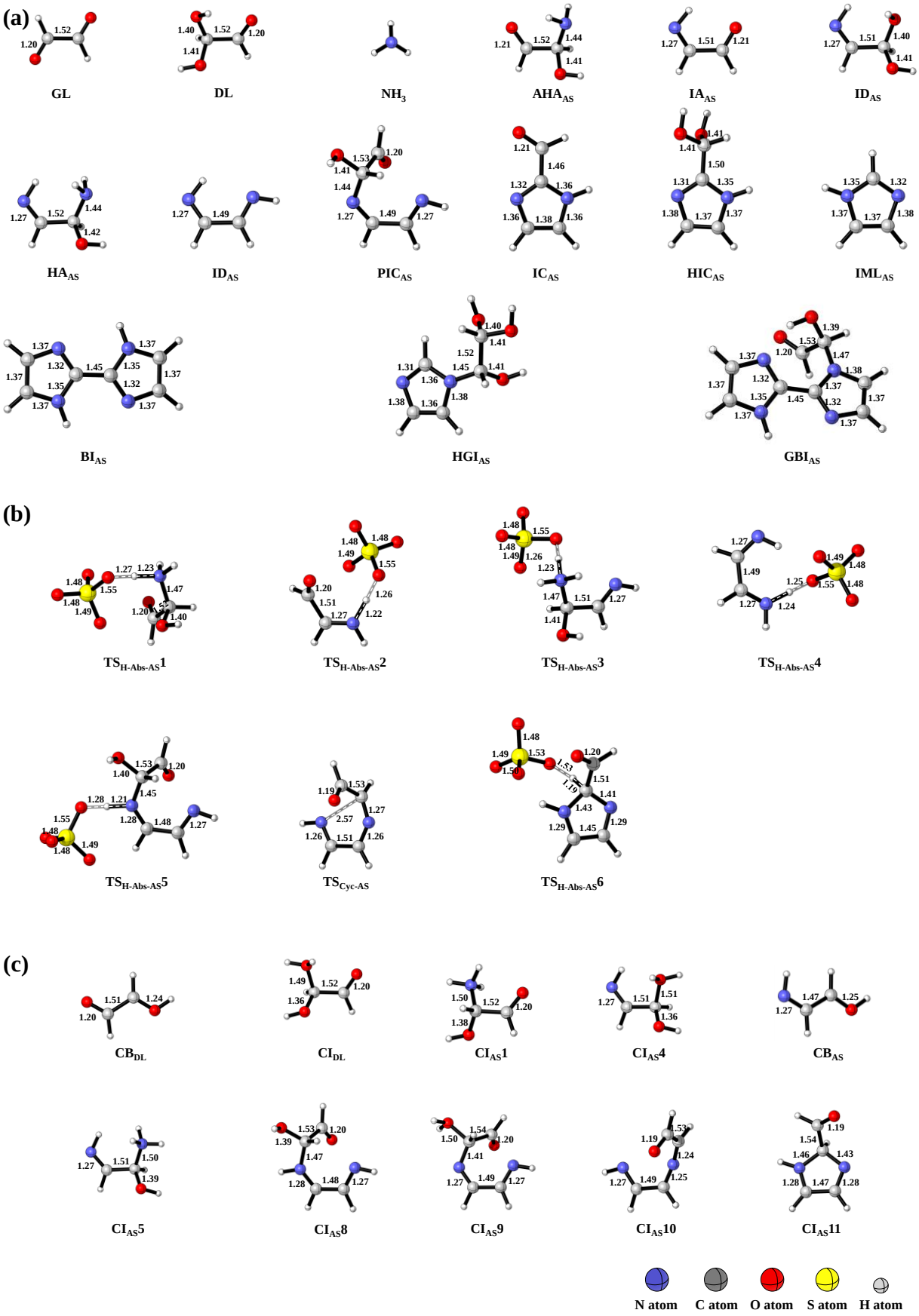

Figure S10. The optimized geometries of SPs including products (a), TSs (b) and CIs(c) in AS-GL mixture.

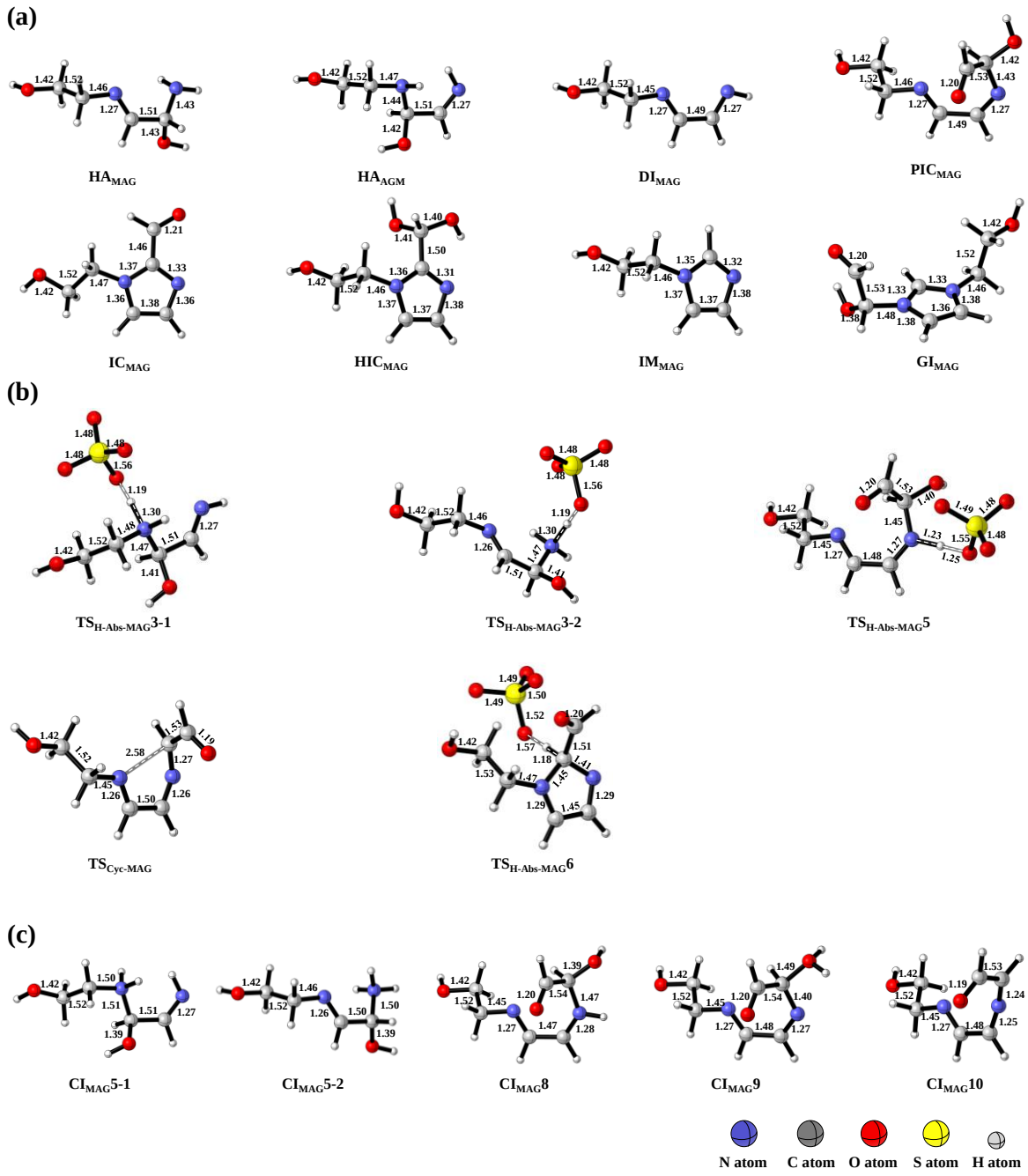

Figure S11. The optimized geometries of SPs including products (a), TSs (b) and CIs(c) in MEA-AS-GL mixture.

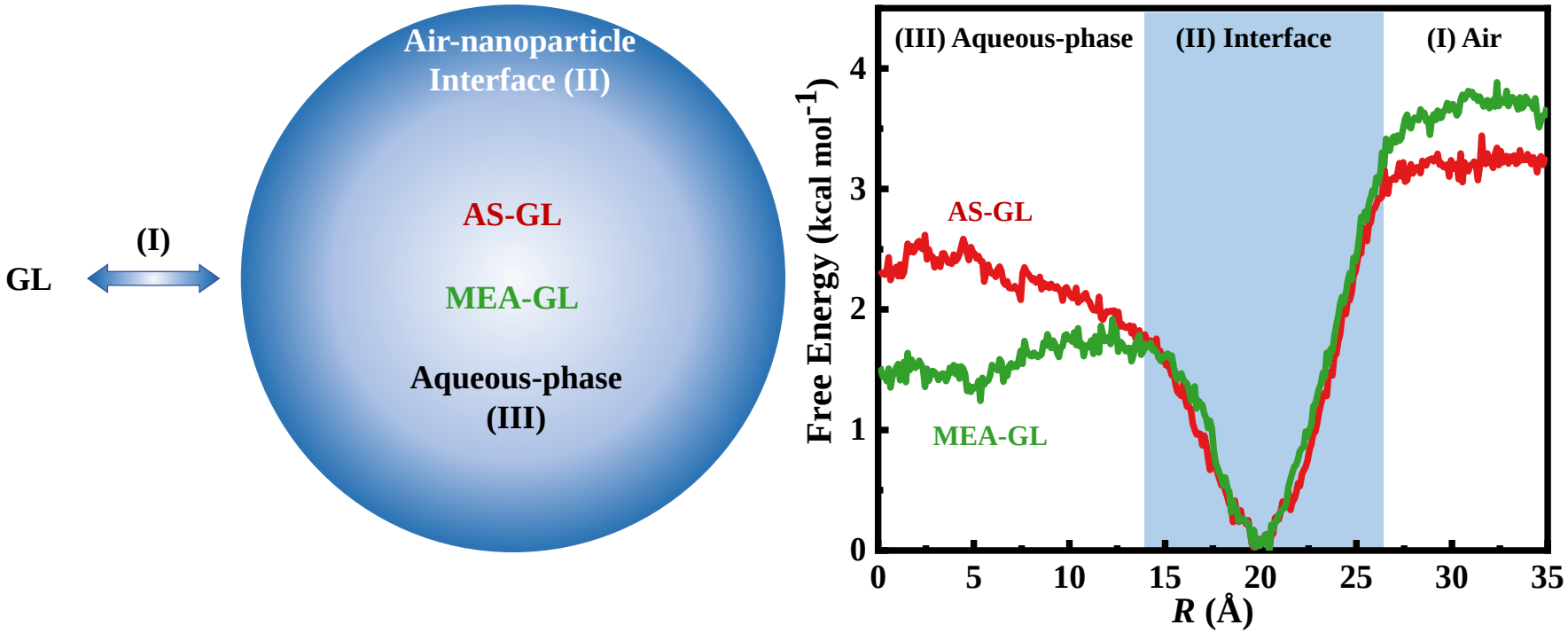

Figure S12. The critical processes of gaseous GL coming into the particles (left) and the free energy profile of gaseous GL approaching the MEA (green line) particle and AS (red line) particle (right).

Table S1. Structures and corresponding formulas, measured m/z values and fragments of products generated in MEA-GL, AS-GL and MEA-AS-GL mixtures.

Formulas	Measured m/z values (+ H^+)	Fragments (+ H^+)	Structures	Mixture	Name
$C_3H_4N_2$	69.045	-		AS-GL MEA-AS-GL	IML_{AS}
$C_4H_4N_2O$	97.040	**69.045**		AS-GL MEA-AS-GL	IC_{AS}
$C_4H_6N_2O_2$	115.050	**97.040** 69.045	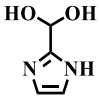	AS-GL	HIC_{AS}
$C_6H_6N_4$	135.067	**81.045** 108.056	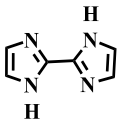	AS-GL	BI_{AS}
$C_5H_8N_2O_3$	145.060	**127.050** 109.040 81.045	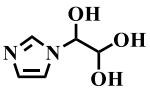	AS-GL	HGI_{AS}
$C_8H_8N_4O_2$	193.072	**135.066** 81.045	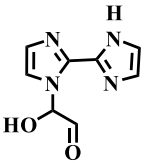	AS-GL	GBI_{AS}
$C_5H_8N_2O$	113.071	**69.045** 95.061		MEA-AS-GL	IML_{MAG}
$C_6H_8N_2O_2$	141.066	**123.055** 97.040 69.045	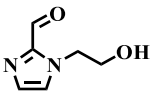	MEA-AS-GL	IC_{MAG}
$C_6H_{10}N_2O_3$	159.076	**141.066** 97.040 69.045	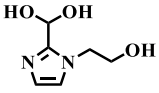	MEA-AS-GL	HIC_{MAG}
$C_7H_{11}N_2O_3$	171.076	**103.039** 113.071 69.045	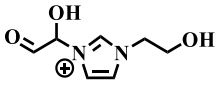	MEA-AS-GL	GI_{MAG}
$C_4H_9NO_3$	120.066	**74.061** 56.050 102.055	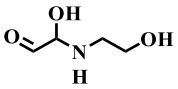	MEA-GL MEA-AS-GL	AHA_{MEA}
$C_4H_7NO_2$	102.055	**56.050** 74.060		MEA-GL MEA-AS-GL	IA_{MEA}
$C_4H_9NO_3$	120.066	**74.060** 56.050 102.055	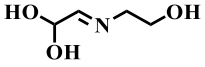	MEA-GL MEA-AS-GL	ID_{MEA}

Formulas	Measured m/z values (+ H^+)	Fragments (+ H^+)	Structures	Mixture	Name
$C_7H_{13}N_2O_2$	157.097	**113.071** 69.045		MEA-GL MEA-AS-GL	IML_{MEA}
$C_8H_{13}N_2O_3$	185.092	**141.065** 97.040 113.071	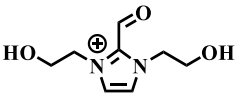	MEA-GL MEA-AS-GL	IC_{MEA}
$C_8H_{15}N_2O_4$	203.102	**157.097** 113.071 69.045	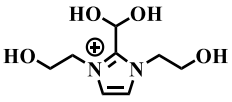	MEA-GL	HIC_{MEA}

*The fragments are ordered by intensity in descending and the ones with the most abundant intensity are written in bold.

Table S2. Average pH values of all reaction systems with initial pH 3 or 4 over a time scale of 15 d.

Reaction Time (d)	AS-GL (pH3)	AS-GL (pH4)	MEA-GL (pH3)	MEA-GL (pH4)	MEA-AS-GL (pH3)	MEA-AS-GL (pH4)
Initial pH	3.01	4.02	3.01	3.97	3.03	3.99
1	2.55	2.64	2.22	2.32	1.81	1.93
2	2.39	2.46	2.00	1.98	1.71	1.81
3	2.31	2.37	1.85	1.87	1.62	1.75
5	2.21	2.26	1.69	1.67	1.51	1.65
7	2.15	2.20	1.59	1.65	/	1.60
9	2.09	2.14	1.52	1.55	1.56	1.59
11	2.07	2.12	1.55	1.56	1.54	1.53
13	2.03	2.08	1.50	1.55	1.52	1.53
15	2.03	2.07	1.47	1.48	1.49	1.55

Table S3. The activation barrier energies ($\Delta G^{\ddagger}$), the reaction energy (ΔG_r), and the rate constants (k) for the protonation pathways from N-containing CIs. Herein, the units of energies and rate constants are kcal mol^{-1} and M^{-1} s^{-1}, respectively.

Reactions	$\Delta G^{\ddagger}$	ΔG_r	k
MEA-GL mixture:			
$GL + MEA \rightarrow Add_{MEA}$	6.3	6.4	2.68×10^8
$Add_{MEA} \rightarrow AHA_{MEA}$	15.2	-13.9	[b]38
$CI_{MEA}1 + SO_4^{2-} \rightarrow AHA_{MEA} + HSO_4^-$	-4.5	-7.7	1.27×10^9
$CI_{MEA}5 + SO_4^{2-} \rightarrow HA_{MEA} + HSO_4^-$	-2.3	-5.3	1.16×10^9
$CI_{MEA}8 + SO_4^{2-} \rightarrow PIC_{MEA} + HSO_4^-$	17.5	-0.2	1.74
AS-GL mixture:			
$GL + NH_3 \rightarrow Add_{AS}$	8.6	5.8	5.78×10^6
$Add_{AS} \rightarrow AHA_{AS}$	18.2	-11.9	[b]2.48×10^{-1}
$CI_{AS}1 + SO_4^{2-} \rightarrow AHA_{AS} + HSO_4^-$	-3.4	-7.0	1.41×10^9
$CI_{AS}5 + SO_4^{2-} \rightarrow HA_{AS} + HSO_4^-$	-5.3	-7.5	1.40×10^9
$CI_{AS}8 + SO_4^{2-} \rightarrow PIC_{AS} + HSO_4^-$	-5.0	-12.4	1.34×10^9
$CI_{AS}10 \rightarrow CI_{AS}11$	3.9	-33.5	[a]3.03×10^{10} [b]8.35×10^9
$CI_{AS}11 + SO_4^{2-} \rightarrow IC_{AS} + HSO_4^-$	-0.6	-42.5	1.59×10^9
MEA-AS-GL mixture:			
$CI_{MAG}5\text{-}1 + SO_4^{2-} \rightarrow HA_{AGM} + HSO_4^-$	-6.7	-8.3	1.23×10^9
$CI_{MAG}5\text{-}2 + SO_4^{2-} \rightarrow HA_{MAG} + HSO_4^-$	-0.8	-4.4	1.23×10^9
$CI_{MAG}8 + SO_4^{2-} \rightarrow PIC_{MAG} + HSO_4^-$	-5.4	-11.3	1.26×10^9
$CI_{MAG}10 \rightarrow CI_{MAG}11$	5.0	-32.8	[a]4.15×10^9 [b]1.29×10^9
$CI_{MAG}11 + SO_4^{2-} \rightarrow IC_{MAG} + HSO_4^-$	1.6	-39.4	1.61×10^9

Calculated via [a]Kisthelp or [b]script.

References

Collins, F. C. and Kimball, G. E.: Diffusion-controlled reaction rates, J. Colloid Sci., 4, 425-437, https://doi.org/10.1016/0095-8522(49)90023-9, 1949.

CYLview, b. L., C. Y., Université de Sherbrooke, 2009 (http://www.cylview.org): [code],

Einstein, A.: Über die von der molekularkinetischen Theorie der Wärme geforderte Bewegung von in ruhenden Flüssigkeiten suspendierten Teilchen, Ann. Phys., 322, 549-560, https://doi.org/10.1002/andp.19053220806, 1905.

Eyring, H.: The Activated Complex in Chemical Reactions, J. Chem. Phys., 3, 107-115, https://doi.org/10.1063/1.1749604, 1935.

Galano, A. and Alvarez-Idaboy, J. R.: Guanosine + OH Radical Reaction in Aqueous Solution: A Reinterpretation of the UV−vis Data Based on Thermodynamic and Kinetic Calculations, Org. Lett., 11, 5114-5117, https://doi.org/10.1021/ol901862h, 2009.

Gao, Y., Ji, Y., Li, G., and An, T.: Mechanism, kinetics and toxicity assessment of OH-initiated transformation of triclosan in aquatic environments, Water Res., 49, 360-370, https://doi.org/10.1016/j.watres.2013.10.027, 2014.

Ji, Y., Shi, Q., Ma, X., Gao, L., Wang, J., Li, Y., Gao, Y., Li, G., Zhang, R., and An, T.: Elucidating the critical oligomeric steps in secondary organic aerosol and brown carbon formation, Atmos. Chem. Phys., 22, 7259-7271, https://doi.org/10.5194/acp-22-7259-2022, 2022.

Okuno, Y.: Theoretical Investigation of the Mechanism of the Baeyer-Villiger Reaction in Nonpolar Solvents, Chem. - Eur. J., 3, 212-218, https://doi.org/10.1002/chem.19970030208, 1997.

Truhlar, D. G.: Nearly encounter-controlled reactions: The equivalence of the steady-state and diffusional viewpoints, J. Chem. Educ., 62, 104, https://doi.org/10.1021/ed062p104, 1985.